Large eddy simulation of compressible turbulent jets

By B. J. Boersma & S. K. Lele

1. Motivation

Increasing noise regulation at urban airports force jet engine manufactures to develop and build quieter engines. Over the last 10-15 years, a significant reduction in fan and mechanical noise has been achieved. However, the reduction in jet noise over the same time period is fairly small and a major reduction in acoustic emissions of jet engines has to come from a reduction in jet noise.

Traditional jet mixing-noise predictions are based on a statistical description of the jet turbulence; space-time correlations of the Lighthill quadruples (Lighthill 1952, Lighthill 1954) are specified in the jet. Further refinements are, however, needed to obtain a reasonable prediction of the directivity and spectral distribution of the radiated noise (Goldstein 1976). Significant improvements are achieved by modeling the effects of source-convection (Lighthill 1954, Ffowcs Williams & Hawkins 1969) and mean-flow refraction (Mani 1976). Reynolds-averaged mean flow calculations can be used to provide the source-strength distribution and the length and time-scale estimates needed in the source models (Bechara *et al.* 1994). The empirical input needed in such an approach places limits on the range of applicability of this method. It is, therefore, desirable to develop methods which obtain the unsteady flow data with much less empirical input.

Due to the inherently high Reynolds numbers of the jet formed by a jet engine, LES seems to be the only feasible candidate to obtain the necessary unsteady data for the jet. Some attempts for round jets have been made by Choi *et al.* (1999) and Boersma & Lele (1999). For simpler geometries like plane mixing layers, various simulations have also been performed by Vreman *et al.* (1996).

In this paper we will describe an LES method which uses the standard compressible LES filtered variables (no Favre averaging). The LES equation are discretized with accurate numerical schemes with very little artificial diffusion. So the LES models have to supply all the damping of the non-linear terms. In LES models which use low order numerics, damping can come from the LES subgrid model or from the numerics, and it is often very difficult to separate those two effects. This makes the physical interpretation of the results, especially those related to subgrid motions, difficult.

2. Large eddy simulation

In most LES of compressible flows, the flow variables are Favre averaged or density weighted

$$\tilde{f} = \frac{\overline{\rho f}}{\overline{\rho}} \tag{1}$$

where the bar denotes the standard LES filtering and ρ the density. Using the Favre average and applying the standard LES filtering technique, we find the following equation for conservation of mass

$$\frac{\partial \overline{\rho}}{\partial t} + \frac{\partial}{\partial x_i}(\overline{\rho}\tilde{u}_i) = 0, \tag{2}$$

in which u_i is the fluid velocity vector. Conservation of momentum reads

$$\frac{\partial \overline{\rho}\tilde{u}_i}{\partial t} + \frac{\partial}{\partial x_i}(\overline{\rho}\tilde{u}_i\tilde{u}_j) = -\frac{\partial \overline{p}}{\partial x_i} + \frac{\partial}{\partial x_j}\tilde{\sigma}_{ij} - \frac{\partial}{\partial x_j}\overline{\rho}(\widetilde{u_i u_j} - \tilde{u}_i\tilde{u}_j) \tag{3}$$

in which p is the pressure and $\tilde{\sigma}_{ij}$ is the viscous stress tensor, which is defined as

$$\tilde{\sigma}_{ij} = \overline{\mu}\left(\frac{\partial \tilde{u}_i}{\partial x_j} + \frac{\partial \tilde{u}_j}{\partial x_i} - \frac{2}{3}\delta_{ij}\frac{\partial \tilde{u}_k}{\partial x_k}\right) \tag{4}$$

where $\overline{\mu}$ denotes the kinematic viscosity, and δ_{ij} denotes the Kronecker delta function. For the energy equation several variants are possible. We follow Freund *et al.* (1997) and use the following equation

$$\frac{\partial \overline{E}}{\partial t} + \frac{\partial}{\partial x_i}\left(\tilde{u}_i(\overline{E} + \overline{p}\right) = -\frac{\partial}{\partial x_i}q_i + \frac{\partial}{\partial x_j}(\tilde{\sigma}_{ij}\tilde{u}_i) - \frac{\partial}{\partial x_i}\left(\overline{Eu_i} - \overline{E}\tilde{u}_i + \overline{pu_i} - \overline{p}\tilde{u}_i\right) \tag{5}$$

$$q_i = -\overline{\kappa}\frac{\partial \tilde{T}}{\partial x_i} \tag{6}$$

where $E = \rho T/\gamma + \rho u_i u_i/2$ is the total energy per unit volume, γ the specific heat ratio, T the temperature, q the heat flux, and κ the thermal diffusivity. Formally, the term $\tilde{u_i}\ \tilde{\sigma}_{ij}$ would also lead to an additional term; however, it is expected that term will be small, and it is, therefore, neglected (see for instance Moin *et al.* 1991)

If we use the LES averaging but without density weighting, we find the following equations for conservation of mass and momentum

$$\frac{\partial \overline{\rho}}{\partial t} + \frac{\partial \overline{\rho}\ \overline{u}_i}{\partial x_i} = -\frac{\partial}{\partial x_i}\left(\overline{\rho u_i} - \overline{\rho}\ \overline{u}_i\right), \tag{7}$$

$$\frac{\partial \overline{\rho}\ \overline{u}_i}{\partial t} + \frac{\partial \overline{\rho}\ \overline{u}_i\ \overline{u}_j}{\partial x_j} = -\frac{\partial \overline{p}}{\partial x_i} + \frac{\partial \overline{\sigma}_{ij}}{\partial x_j} - \frac{\partial}{\partial x_j}\left(\overline{\rho u_i u_j} - \overline{\rho}\ \overline{u}_i\ \overline{u}_j\right) - \frac{\partial}{\partial t}\left(\overline{\rho u_i} - \overline{\rho}\ \overline{u}_i\right) \tag{8}$$

In which $\overline{\sigma}_{ij}$ is the Newtonian stress tensor

$$\overline{\sigma}_{ij} = \overline{\mu}\left(\frac{\partial \overline{u}_i}{\partial x_j} + \frac{\partial \overline{u}_j}{\partial x_i} - \frac{2}{3}\delta_{ij}\frac{\partial \overline{u}_k}{\partial x_k}\right) \tag{9}$$

The LES filtered equation for the total energy reads

$$\frac{\partial \overline{E}}{\partial t}+\frac{\partial}{\partial x_i}[\overline{E}\ \overline{u_i}+\overline{u_i}\ \overline{p}]=-\frac{\partial q_i}{\partial x_i}+\frac{\partial}{\partial x_i}\overline{u_i}\ \overline{\sigma}_{ij}-\frac{\partial}{\partial x_i}\left(\overline{Eu_i}-\overline{E}\ \overline{u_i}+\overline{pu_i}-\overline{p}\ \overline{u_i}\right). \quad (10)$$

$$q_i=-\overline{\kappa}\frac{\partial \overline{T}}{\partial x_i}$$

In both sets of equations the variables are made non-dimensional using the ambient speed of sound c_∞ as reference velocity scale, the ambient density ρ_∞ as reference density, $\rho_\infty c_\infty^2$ as reference pressure, and c_∞^2/C_p as reference temperature.

From the two sets of equations given above, it is clear that the Favre averaged set is simpler. In the Favre averaged equations, no model is necessary in the continuity equation. The unsteady subgrid term in the momentum equation does not require a new model since it already appears in (7). On the other hand, by using Favre averaging of the governing equation, some information is lost. For relatively low Mach numbers this is not really a problem, see e.g. Freund *et al.* (1997), where the differences between two types of averaging was found to be small for mixing layer flows.

However, the Favre averaged continuity equation is still a non-linear equation which can cause numerical instabilities. We indeed observed such instabilities leading to small grid point to grid point waves. These waves have to be removed from the flow field. This can be done by adding an artificial diffusion term to the right-hand side of the continuity equation. Another way to do this is by using the non Favre averaged LES equations. In this set of equations a damping term is already present in the continuity equation. We have chosen this latter approach because we feel that it is closer to the physics of the problem. On the other hand, the LES modeling of the non-Favre averaged equations is a little bit more complicated due to the appearance of an additional unsteady term in the momentum equation. The subgrid mass terms in the momentum and density equation will not lead to an additional sound source because those terms vanish when one derives the Lighthill equation from the non-Favre averaged density and momentum equations.

LES models

The new unknowns which arise due to the LES filtering of the governing equations have to be modeled. In this section we will give some models for these unknowns. The model parameters in these models are calculated with the dynamic procedure (Germano 1991). With help of the Boussinesq hypothesis, we can write the following simple model for the subgrid mass flux:

$$m_i=\overline{\rho u_i}-\overline{\rho}\ \overline{u}_i=-C_\rho\Delta^2|\overline{S}|\frac{\partial \overline{\rho}}{\partial x_i} \quad (11)$$

In which Δ is the filter width of the LES filter, and C_ρ a coefficient which is obtained from the dynamic procedure (Germano 1991) and S is the strain rate tensor defined as

$$S_{ij}=\frac{1}{2}\left(\frac{\partial u_i}{\partial x_j}+\frac{\partial u_j}{\partial x_i}\right). \quad (12)$$

For the subgrid stresses we can use again a model based on the Boussinesq hypothesis (see e.g. Moin *et al.* 1991)

$$\overline{\rho u_i u_j} - \overline{\rho}\ \overline{u}_i\ \overline{u}_j = \overline{\rho} C_s \Delta^2 |\overline{S}| \overline{S}_{ij} = \overline{\rho} \nu_t \overline{S}_{ij} \tag{13}$$

in which C_s is the well known Smagorinsky coefficient which is evaluated using the dynamic procedure and ν_t the so-called eddy viscosity.

With the help of the equation of state

$$p = \rho \frac{\gamma - 1}{\gamma} T \tag{14}$$

we can rewrite the subgrid term in the energy equation as

$$\overline{u_i E} + \overline{u_i p} - \overline{u_i}\ \overline{E} - \overline{u_i}\ \overline{p} = \left(\overline{\rho u_i T} - \overline{\rho}\ \overline{u_i}\ \overline{T} + \frac{1}{2} \overline{\rho u_i u_k u_k} - \frac{1}{2} \overline{\rho}\ \overline{u_i}\ \overline{u_k}\ \overline{u_k} \right) \tag{15}$$

It is assumed that the convection of the subgrid kinetic energy by the subgrid velocity is small, so we can write for the right hand side of equation (15):

$$\left(\overline{\rho u_i T} - \overline{\rho}\ \overline{u_i}\ \overline{T} + \frac{1}{2} \overline{\rho u_i u_k u_k} - \frac{1}{2} \overline{\rho}\ \overline{u_i}\ \overline{u_k}\ \overline{u_k} \right) \approx \overline{\rho u_i T} - \overline{\rho}\ \overline{u_i}\ \overline{T} \tag{16}$$

This term is modeled with the following model (see e.g. Moin *et al.* 1991):

$$\overline{\rho u_i T} - \overline{\rho}\ \overline{u_i}\ \overline{T} = -\overline{\rho} \frac{\nu_t}{Pr_t} \frac{\partial \overline{T}}{\partial x_i} \tag{17}$$

In which Pr_t is the turbulent Prandtl number which can be calculated dynamically and $\nu_t = C_s \Delta^2 |\overline{S}|$ is the turbulent eddy viscosity of equation (13). Actually we do not calculate Pr_t, but define a new parameter $C_T = C_s / Pr_t$ and calculate this parameter dynamically.

The dynamic procedure

For completeness we will describe the dynamic procedure for the density equation in this section. Dynamic procedures for momentum and energy can be found in Moin *et al.* (1991). The basic assumption in the dynamic procedure is that the closure model for the density equation is valid on the length scale of the LES filter but also for a filter which has a larger filter length. We will call this larger filter the test filter, and test filtered quantities will be denoted by a caret. The test filtered subgrid mass flux is thus given by

$$M_i = \widehat{\overline{\rho u_i}} - \hat{\overline{\rho}}\ \hat{\overline{u_i}} \tag{18}$$

Now it follows from the definitions that

$$M_i - \hat{m}_i = \widehat{\overline{\rho}\ \overline{u_i}} - \hat{\overline{\rho}}\ \hat{\overline{u_i}} \tag{19}$$

This term is computable from the resolved field. If we now use for M_i and m_i the model proposed previously, with the same constant on both filter widths we can derive the following relation for C_ρ

$$\widehat{\overline{\rho}\,\overline{u_i}} - \hat{\overline{\rho}}\,\hat{\overline{u_i}} = -C_\rho \left(\hat{\Delta}^2 |\hat{\overline{S}}| \frac{\partial \hat{\overline{\rho}}}{\partial x_i} - \Delta^2 \widehat{|\overline{S}| \frac{\partial \overline{\rho}}{\partial x_i}} \right) \tag{20}$$

Both the left- and right-hand side of this equation can be computed from the resolved field and C_ρ can be obtained.

For the momentum and energy equations, similar procedures are used by Moin *et al.* (1991). Due to the averaging in the azimuthal direction of the jet, it is not necessary to clip the model parameters C_ρ, C_s, and C_T.

3. Numerical method and boundary conditions

In this section we will give a short overview of the numerical method and boundary conditions which have been used in the simulations.

In this study we use the Navier-Stokes equations rewritten in a cylindrical coordinate system, with x, r, and θ as the axial, radial, and azimuthal coordinate directions, respectively. The numerical scheme is very similar to the one used by Freund *et al.* (1997). Spatial derivatives in axial and radial direction are taken with 6th order compact finite differences (Lele 1992). In the azimuthal direction a Fourier method with approximate dealiasing has been used. To minimize the aliasing error in the radial and axial directions, the non-linear terms have been rewritten in the skew symmetric form, i.e.

$$\frac{\partial \rho u_i u_j}{\partial x} = \frac{1}{2} \left(\frac{\partial \rho u_i u_j}{\partial x} + u_i \frac{\partial \rho u_j}{\partial x} + \rho u_j \frac{\partial u_i}{\partial x} \right) \tag{21}$$

The spatial discretization method given above has almost no artificial numerical dissipation.

The time integration has been carried out with a fourth order Runge-Kutta scheme. Normally, the small grid spacing near the centerline of the cylindrical system would place a severe restriction on the time step of the Runge-Kutta scheme. This problem is avoided by dropping Fourier modes close to the centerline (Freund *et al.* 1997).

At the boundaries of the computational domain, the so-called sponge layers are used to force the flow to a certain *a priori* specified target solution. In this study we use as target solution the self-similarity solution for an incompressible jet.

A point of concern related to the high order numerical schemes such as the ones used in this study is that the discretization does not numerically conserve kinetic energy for an in viscid low Mach number flow. This means that the calculation can become unstable when a flow scale is under-resolved, and there is not enough viscosity (molecular or subgrid) to damp this instability. Because in a LES setting the molecular viscosity is relatively low, all the damping has to come from the

subgrid model. The calculation of the subgrid stresses is subject to numerical errors to the point that $2\Delta x_i$ error waves become apparent. These $2\Delta x_i$ waves in the subgrid stresses can generate instabilities in the resolved quantities. To avoid numerical problems such errors waves are removed by filtering the strain rate tensor S_{ij} before the terms in the subgrid stress are calculated. For this we use the following simple filter (Lele 1992)

$$f_i := \frac{1}{16}\left(-f_{i-2} + 4f_{i-1} + 10f_i + 4f_{i+1} - f_{i+2}\right) \tag{22}$$

in all three coordinate directions. Note that the resolved variables $\overline{\rho}$, $\overline{u_i}$ and $\overline{E}$ are **not** altered by this filtering procedure. Only the subgrid terms which appear after LES-filtering are affected by this procedure. The chosen filter has a truncation error of fourth order, which is much smaller than the error made by using the gradient hypothesis to obtain the subgrid stresses. The code has been implemented on parallel computers using the message passing interface (MPI) and is typically run on 32-64 CPU's.

Inflow conditions

Good inflow conditions for LES and DNS are in general very difficult because time dependent data with appropriate length and time scales have to be supplied. Such information can, for instance, be obtained from a temporal mixing layer calculation. A field of such a calculation can be fed into the computational domain. In such a case we additionally have to specify a convection velocity, and we also have to apply some random forcing to "break" the periodicity of the temporal calculation. Presently, we are mainly interested in getting the LES models working and getting numerically smooth fields. Therefore, we use at the moment a much simpler forcing which is described below.

In the jet inflow plane the following velocity profile is specified

$$u_x(0, r, \theta, t) = Ma\left(\frac{1}{2} - \frac{1}{2}\tanh\left[2.8\left(\frac{r}{R_0} - \frac{R_0}{r}\right)\right]\right)(1 + \epsilon\sin[St\ t]) \tag{23}$$

In which the Strouhal number $St = 2R_0 f/U$ is 0.45 and the amplitude ϵ is 0.0025. To trigger three-dimensional instabilities, a very small random forcing is applied in the circumferential direction in the initial shear layer

$$u_\theta(0, r, \theta) = 0.025\exp[-3(1-r)^2]ran \tag{24}$$

where ran is random number generated uniformly between -0.5 and 0.5. The velocity component in the radial direction is set to zero ($u_r = 0$).

4. Results

In this section we will present some results of the LES of a compressible Mach 0.9 jet. Various runs at different Reynolds numbers have been carried out. We

Table 1. Some parameters used in the simulations.

	I	II
Re	$36,000$	100,000
$N_x \times N_r \times N_\theta$	$192 \times 128 \times 64$	$320 \times 150 \times 96$
L_x	$45R_0$	$47.5R_0$
L_r	$8R_0$	$11R_0$
Δx_{max}	$0.42R_0$	$0.15R_0$
Δx_{min}	$0.14R_0$	$0.15R_0$
Δr_{max}	$0.1R_0$	$0.09R_0$
Δr_{min}	$0.03R_0$	$0.03R_0$

will present results of two runs, one with a moderate Reynolds number (36,000) for which the statistics are more or less converged and one with a high Reynolds number (100,000) but not yet converged statistics. The number of grid points in the moderate Reynolds simulations is equal to $192 \times 128 \times 64$ points in the axial, radial, and circumferential direction respectively. In the high Reynolds number a finer grid with $320 \times 150 \times 96$ points is used (for more details see Table 1). First we will show some statistics obtained from the moderate Reynolds simulations, mainly to validate our LES model.

In Fig. 1 we show the centerline velocity obtained from the medium Reynolds number calculation ($Re = 36 \cdot 10^3$). In this figure we also show the centerline velocity obtained from a DNS carried out by Freund (1999) and experimental data reported by Stromberg *et al.* (1980). There are some small differences between the data sets. These differences are probably due to differences in inlet conditions. In general the agreement between the data sets is quite good.

In Fig. 2 the mean axial velocity profiles obtained from DNS ($Re = 3,600$) and LES ($Re = 36,000$) are plotted. There are again some small differences between the results of the DNS and LES, but the overall picture is quite good. For large radii where the LES and DNS results show some differences, this is most likely due to a difference in the size of the computational domain in the radial direction (the DNS domain is considerably bigger than the LES domain).

In Fig. 3 we show a plot of the Reynolds shear stress $\overline{u_r' u_z'}$ as a function of the radial coordinate at various downstream locations. Again, the agreement between the results obtained from the DNS and LES is reasonable.

Next, some preliminary results obtained from the high Reynolds number ($Re =$ 100.000) calculation will be presented. The statistics of this calculation are not yet converged, and, therefore, we will not show mean profiles, but only instantaneous snapshots and time series.

In Fig. 4 we show a contour plot of the density and total vorticity multiplied by the axial distance x. Due to the relative low Mach number, the variation in density is relatively small. The potential core of the jet breaks up quite far downstream of the

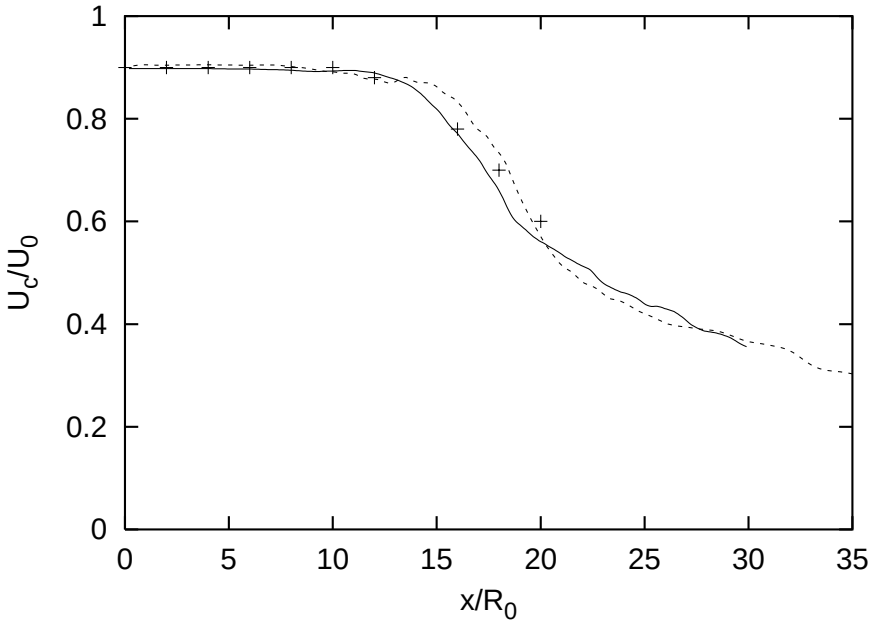

FIGURE 1. The mean centerline velocity as a function of the axial coordinate x, obtained from the LES, DNS (Freund 1999), and experiment (Stromberg *et al.* 1980). DNS 3600: ——— ; Stromberg *et al.* : + ; LES 36000: – – – – .

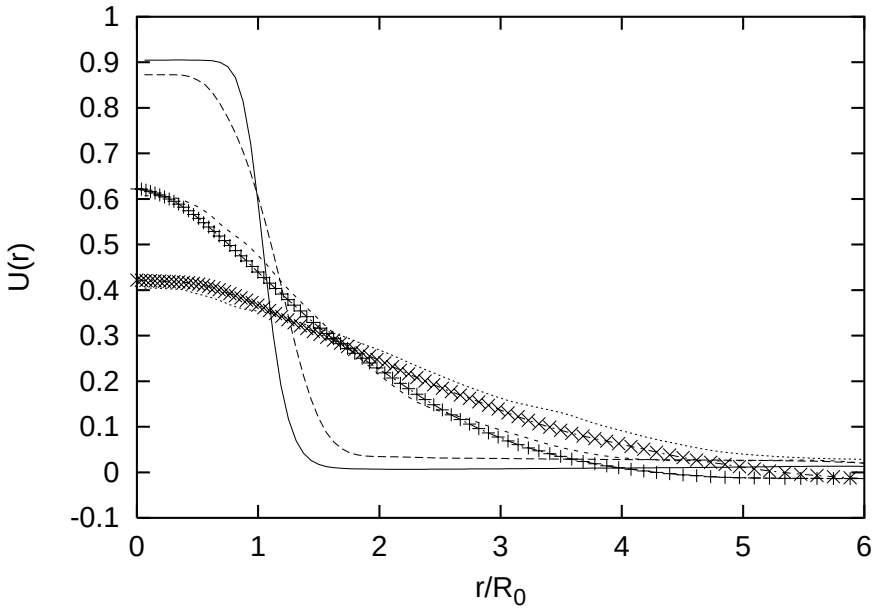

FIGURE 2. The mean velocity as a function of the radial coordinate at various different downstream positions. LES: $x = 3.2R_o$, ——— ; $x = 13.0R_o$, – – – ; $x = 19.5R_o$, – – – – ; $x = 25.9R_o$, ····· . DNS: $x = 19.5R_o$, smallplus; $x = 25.9R_o$, $\times$.

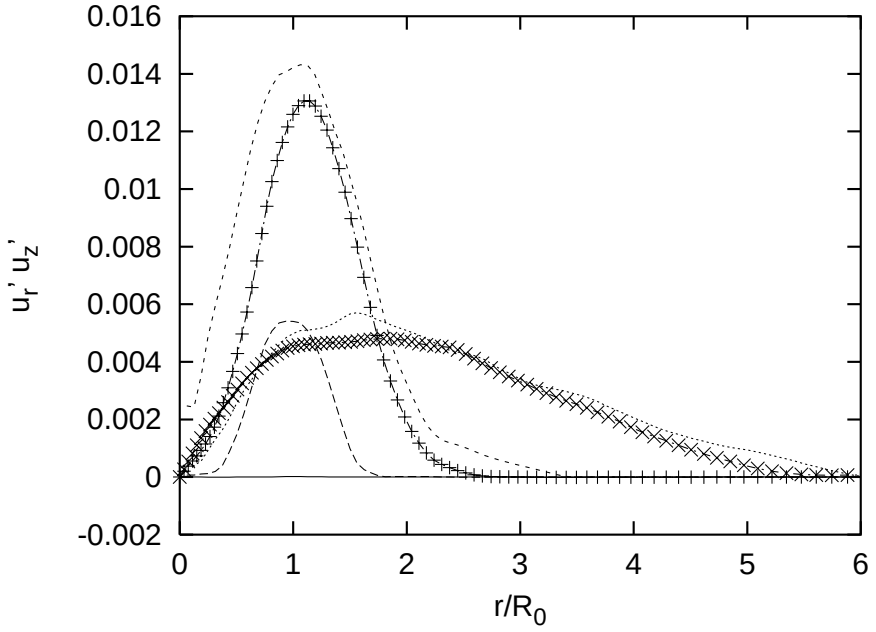

FIGURE 3. The Reynolds shear stress profiles as a function of the radial coordinate obtained at various different downstream positions. LES: $x = 3.2R_o$, ——— ; $x = 13.0R_o$, — — — ; $x = 19.5R_o$, - - - - ; $x = 25.9R_o$, ····· . DNS: $x = 19.5R_o$, smallplus; $x = 25.9R_o$, $\times$.

orifice. This is due to the low amplitude of ϵ in equation (23). A higher amplitude would lead to an earlier breakup but also to a generation of high amplitude pressure waves at the jet orifice. These waves will contaminate the acoustic field. Therefore, ϵ should be kept as small as possible.

The final goal of this research is to obtain the sound field of the jet. A good measure for the sound waves emitted by a flow is the dilatation (or divergence of the velocity). In Fig. 5 the dilatation is plotted. It is clear that in the region where the potential core breaks up sound waves are produced. Furthermore, it is clear that at the jet orifice also sound is produced. This is purely due to the perturbation we use in the inflow velocity profile (Eq. 23) of the jet.

In Fig. 6 we show time series of the pressure at the points ($r = 6.6R_0, x = 11.2R_0$), $(6.6, 16.8)$, $(6.6, 22.4)$, $(6.6, 28.1)$, $(6.6, 33.8)$. The pressure series taken close to the jet inflow plane show much less fluctuations than the points further downstream of the orifice. Close to the jet orifice, the perturbation defined by Eq. (23) is visible in the pressure signals. In the signals farther downstream, the perturbation is no longer visible.

In Fig. 7 we show the power spectra of three of the time series shown in Fig. 6. In the signal close to the jet orifice, we observe a peak at a frequency of 0.45, which is exactly the Strouhal number we used in Eq. (23). It seems that, in the far field of the jet, frequencies around $1U_c/R_o$ are preferred and that pressure fluctuations with a frequency above $2U_c/R_o$ are not present.

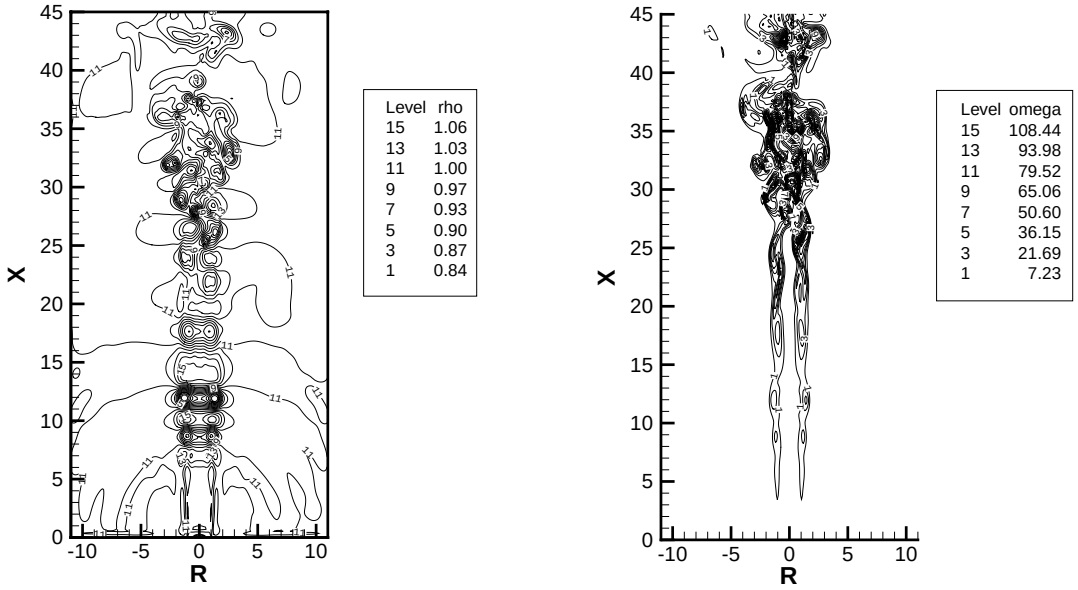

FIGURE 4. Left: Contour plot of the density; Right: Contour plot of the total vorticity multiplied by the axial coordinate $x|\omega|$.

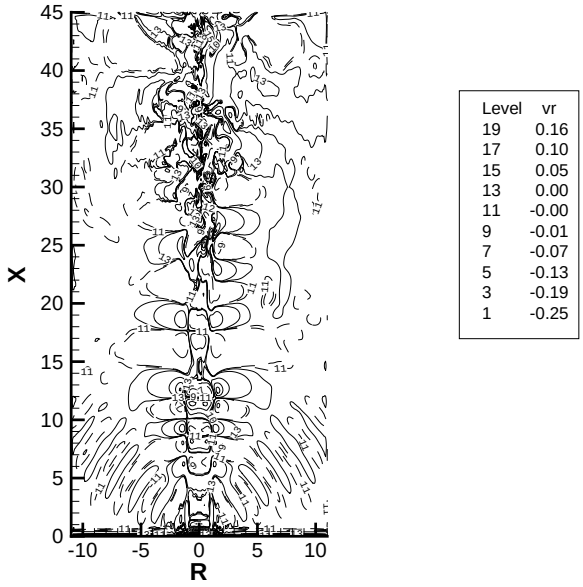

FIGURE 5. A contour plot of the dilatation ($\partial u_i/\partial x_i$).

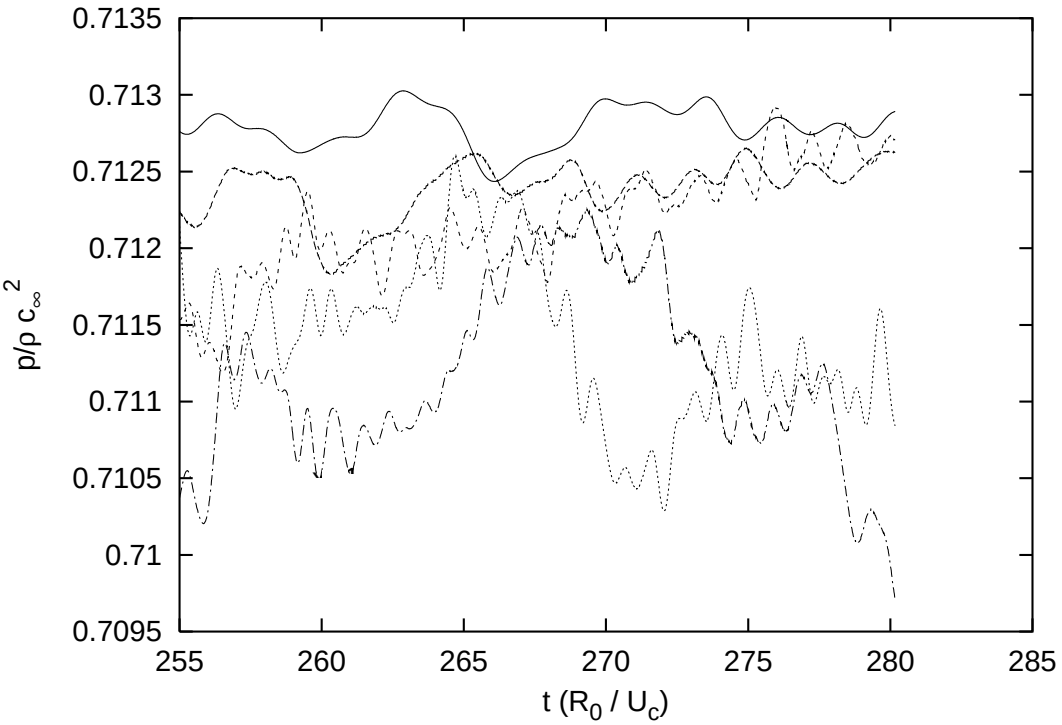

FIGURE 6. Time series of the pressure at the points: $(r = 6.6R_0, x = 11.2R_0)$, ——— ; $(6.6, 16.8)$, — — — ; $(6.6, 22.4)$, - - - - ; $(6.6, 28.1)$, ····· ; $(6.6, 33.8)$, —·— .

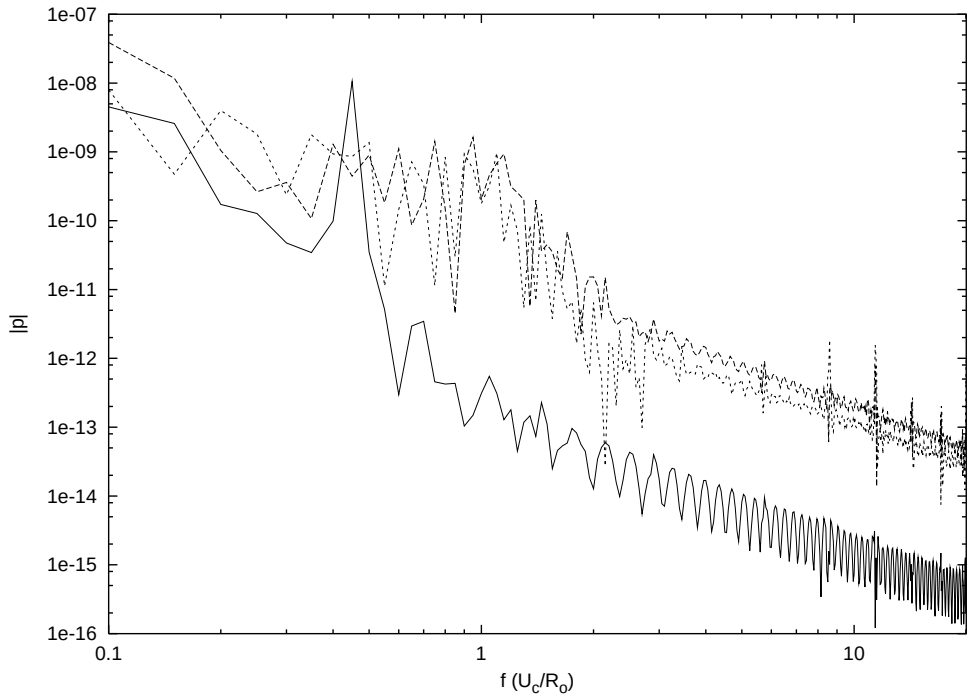

FIGURE 7. Power spectra of the pressure signal at points (r, x): $(6.6, 11.2)$, ——— ; $(6.6, 28.1)$, — — — ; and $(6.6, 33.8)$, - - - - .

Future work

In this paper we have described an LES model for compressible jet flows using high order numerics. The results of a Mach 0.9 jet simulation have been compared with experiments and also with results of direct numerical simulations (DNS). In general the agreement between LES and DNS is reasonable. A high Reynolds number LES simulation is under way. The first results of this simulation look very promising.

Future work will focus on: (1) A more extensive validation of the LES by comparing it to high Reynolds number jet experiments which are currently being carried out or will be carried out in the near future. (2) The calculation of the far field noise using a Kirchoff surface. (3) Improvement of the inflow conditions.

Acknowledgments

The authors would like to thank Prof. J. Freund for providing the compressible Navier-Stokes solver and for sharing his DNS results prior to their publication. This work was supported, in part, by NASA grants NAG 2-1213 and NAG 2-1373.

REFERENCES

Bechara, W., Bailly, C., Lafon, P., Candel, S. 1994 Stochastic approach to noise modeling for free turbulent flows. *AIAA J.* **32,** 455-463.

Boersma, B. J. & Lele, S. K. 1999 Large eddy simulation of Mach 0.9 compressible jet. *AIAA paper 99-1874.*

Choi, D., Barber, T. J., & Chiappetta, L. M. 1999 Large eddy simulation of High-Reynolds number jet flows. *AIAA paper 99-0230.*

Ffowcs Williams, J. E. & Hawkins, D. L. 1969 Sound generated by turbulence and surfaces in arbitrary motion. *Proc. of Roy Soc. of London.* **264,** 321-342.

Freund, J. B. 1997 A proposed inflow/outflow boundary condition for direct computation of aerodynamic sound. *AIAA J.* **35,** 740-742.

Freund, J. B. 1999 Acoustic sources in a turbulent jet: a direct numerical simulation study. *AIAA paper 99-1858.*

Freund, J. B., Moin, P. & Lele, S. K. 1997 Compressibility effects in a turbulent annular mixing layer. *Tech. Rep. TF-72.* Flow Physics & Computation Division, Dept. of Mechanical Engineering, Stanford University.

Germano, M., Piomelli, U., Moin, P. & Cabot, W. 1990 dynamic subgrid-scale eddy viscosity model. *Proceedings of the 1990 Summer Program.* Center for Turbulence Research, NASA/Stanford Univ. 5-17.

Goldstein, M. E. 1976 Aeroacoustics. McGraw Hill.

Lele, S. K. 1992 Compact finite difference schemes with spectral-like resolution. *J. Comp. Phys.* **103,** 16-42.

Lighthill, M. J. 1952 On sound generated aerodynamically. *Proc. R. Soc. of London Ser. A.* **211,** 564-587.

Lighthill, M. J. 1954 On sound generated aerodynamically: II. Turbulence as a source of sound. *Proc. R. Soc. of London, Ser. A.* **222,** 1-32.

Mani, R. 1976 The influence of jet flow on jet noise. Part I. The noise of unheated jets. *J. Fluid Mech.* **73,** 753-778.

Moin, P., Squires, K., Cabot, W. & Lee, S. 1991 A dynamic subgrid-scale model for compressible turbulence and scalar transport. *Phys. Fluids A.* **3,** 2746-2757.

Nelson, C. & Menon, S. 1998 Unsteady simulations of compressible spatial mixing layers. *AIAA paper 98-0786.*

Stromberg, J. L., McLaughlin, D. K., & Troutt, T. R. 1980 Flow field and acoustic properties of a Mach number 0.9 jet at low Reynolds number. *J. of Sound & Vib.* **72,** 159-176.

Vreman, B. 1996 Direct and large-eddy simulation of the compressible mixing layer, *PhD Thesis,* University of Twente, The Netherlands.